UNIVERSITÀ DEGLI STUDI DI BARI ALDO MORO
DIPARTIMENTO INTERATENEO DI FISICA
INFN Istituto Nazionale di Fisica Nucleare
Quasimodo Quantum sensing for one-health

# Grokking as an entanglement transition during training dynamics of MPS machine learning

Domenico Pomarico

October 29, 2024

Quantum Computing @ INFN, Padova

# Outline

- Tensor Networks
  - Matrix Product State (MPS)
  - Gradient descent
- Fashion MNIST
  - Features extraction in magnetization patterns
  - Entanglement transition
- Gene communities
  - Dataset $\&$ workflow
  - MPS classification

# Outline

- Tensor Networks
  - Matrix Product State (MPS)
  - Gradient descent
- Fashion MNIST
  - Features extraction in magnetization patterns
  - Entanglement transition
- Gene communities
  - Dataset & workflow
  - MPS classification

# Matrix Product State (MPS)

Qubits encoding: features vector $\mathbf{x} \in \mathbb{R}^N \mapsto |\Phi(\mathbf{x})\rangle = \bigotimes_{j=1}^{N} |\phi(x^{(j)})\rangle \in \mathbb{R}^{2^N}$

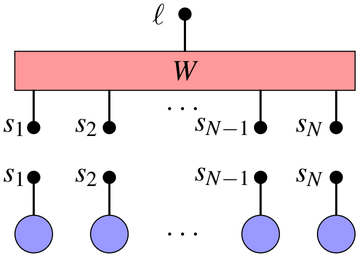


$$f_W^\ell(\mathbf{x}) = \sum_{s_1 \dots s_N} W^\ell_{s_1,\dots,s_N} |\phi(x^{(1)})^{s_1} \dots \phi(x^{(N)})^{s_N}\rangle$$

$$\mathcal{C}(W) = \frac{1}{2} \sum_{\omega=1}^{N_T} \sum_{\ell} \left( f_W^\ell(\mathbf{x}_\omega) - y_\omega^\ell \right)^2$$

# Matrix Product State (MPS)

Qubits encoding: features vector $\mathbf{x} \in \mathbb{R}^N \mapsto |\Phi(\mathbf{x})\rangle = \bigotimes_{j=1}^{N} |\phi(x^{(j)})\rangle \in \mathbb{R}^{2^N}$

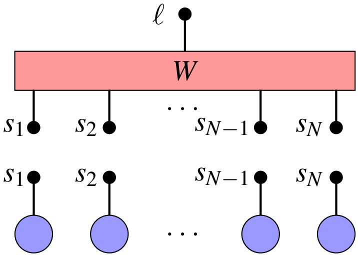


$$f_W^\ell(\mathbf{x}) = \sum_{s_1 \dots s_N} W^\ell_{s_1,\dots,s_N} |\phi(x^{(1)})^{s_1} \dots \phi(x^{(N)})^{s_N}\rangle$$

$$\mathcal{C}(W) = \frac{1}{2} \sum_{\omega=1}^{N_T} \sum_{\ell} \left( f_W^\ell(\mathbf{x}_\omega) - y_\omega^\ell \right)^2$$

MPS format uses iterated *SVD* ($M = U\Sigma V^\dagger$):

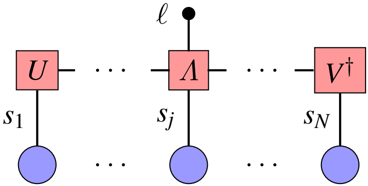


$$W^\ell_{s_1,\dots,s_N} = \sum_{a_1,\dots,a_N} U^{1,a_1}_{s_1} U^{a_1,a_2}_{s_2} \dots U^{a_{j-2},a_{j-1}}_{s_{j-1}} \times$$
$$\times \Lambda^{a_{j-1},a_j}_{s_j,\ell} V^{\dagger a_j,a_{j+1}}_{s_{j+1}} \dots V^{\dagger a_{N-2},a_{N-1}}_{s_{N-1}} V^{\dagger a_{N-1},1}_{s_N}$$

# Matrix Product State (MPS)

Qubits encoding: features vector $\mathbf{x} \in \mathbb{R}^N \mapsto |\Phi(\mathbf{x})\rangle = \bigotimes_{j=1}^{N} |\phi(x^{(j)})\rangle \in \mathbb{R}^{2^N}$

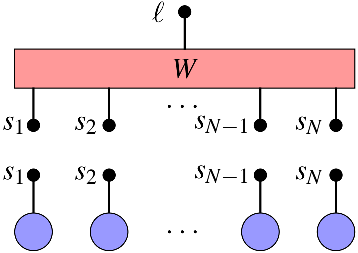


$$f_W^{\ell}(\mathbf{x}) = \sum_{s_1 \dots s_N} W^{\ell}_{s_1,\dots,s_N} \, |\phi(x^{(1)})^{s_1} \dots \phi(x^{(N)})^{s_N}\rangle$$

$$\mathcal{C}(W) = \frac{1}{2} \sum_{\omega=1}^{N_T} \sum_{\ell} \left( f_W^{\ell}(\mathbf{x}_\omega) - y_\omega^{\ell} \right)^2$$

\# singular values $=$ bond dimension $\chi$

MPS format uses iterated *SVD* ($M = U \Sigma V^\dagger$):

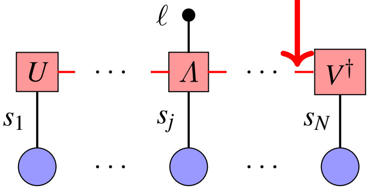


$$W^{\ell}_{s_1,\dots,s_N} = \sum_{a_1,\dots,a_N} U^{1,a_1}_{s_1} U^{a_1,a_2}_{s_2} \dots U^{a_{j-2},a_{j-1}}_{s_{j-1}} \times$$
$$\times \, \Lambda^{a_{j-1},a_j}_{s_j,\ell} V^{\dagger a_j,a_{j+1}}_{s_{j+1}} \dots V^{\dagger a_{N-2},a_{N-1}}_{s_{N-1}} V^{\dagger a_{N-1},1}_{s_N}$$

# Gradient descent

## Two sites update:

$$f_W^\ell(\mathbf{x}) = \sum_{\substack{s_j, s_{j+1} \\ a_{j-1}, a_{j+1}}} B^{a_{j-1}, \ell, a_{j+1}}_{s_j, s_{j+1}} \, |\widetilde{\Phi}(\mathbf{x})^{s_j, s_{j+1}}_{a_{j-1}, a_{j+1}}\rangle$$

$$\Delta B^\ell = -\frac{\partial \mathcal{C}}{\partial B^\ell}$$

$$= \sum_{\omega=1}^{N_T} |\widetilde{\Phi}(\mathbf{x}_\omega)\rangle \otimes (y^\ell_\omega - f^\ell_W(\mathbf{x}_\omega))$$

$$\implies \quad B'^\ell = B^\ell + \alpha \Delta B^\ell$$

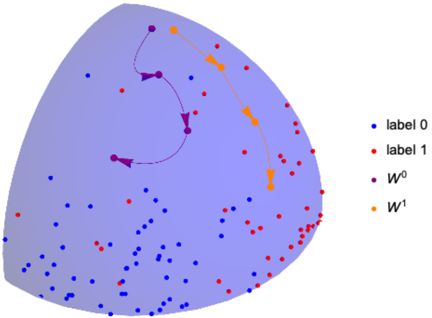


Stoudenmire, Schwab, Supervised Learning with Tensor Networks, 2016

# Gradient descent

## Two sites update:

$$f_W^\ell(\mathbf{x}) = \sum_{\substack{s_j, s_{j+1} \\ a_{j-1}, a_{j+1}}} B^{a_{j-1}, \ell, a_{j+1}}_{s_j, s_{j+1}} \, |\widetilde{\Phi}(\mathbf{x})^{s_j, s_{j+1}}_{a_{j-1}, a_{j+1}}\rangle$$

$$\Delta B^\ell = -\frac{\partial \mathcal{C}}{\partial B^\ell} = \sum_{\omega=1}^{N_T} |\widetilde{\Phi}(\mathbf{x}_\omega)\rangle \otimes (y^\ell_\omega - f^\ell_W(\mathbf{x}_\omega))$$

$$\implies \quad B'^\ell = B^\ell + \alpha \Delta B^\ell$$

$\xrightarrow{SVD}$ entropy $S(j)$

$B'^0 \longrightarrow$ entropy $S^0(j)$

$B'^1 \longrightarrow$ entropy $S^1(j)$

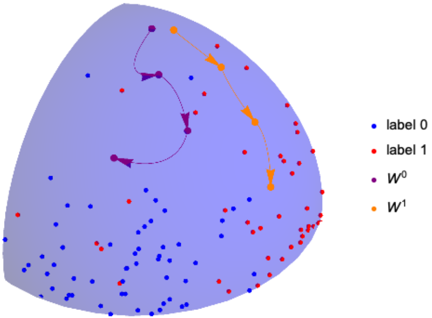


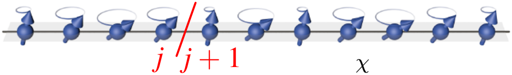


$$S(j) = -\mathrm{Tr}\,\{\varrho_j \log \varrho_j\} = -\sum_{k=1}^{\chi} \lambda_k^2 \log \lambda_k^2$$

Stoudenmire, Schwab, Supervised Learning with Tensor Networks, 2016

# Fashion MNIST

- Tensor Networks
  - Matrix Product State (MPS)
  - Gradient descent
- Fashion MNIST
  - Features extraction in magnetization patterns
  - Entanglement transition
- Gene communities
  - Dataset $\&$ workflow
  - MPS classification

# Fashion MNIST

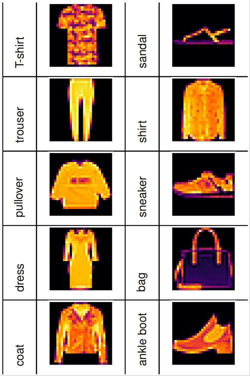


resolution reduction to 6×6 pixels

sneaker binary classifications

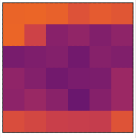

magnetization pattern of quantum masks

grokking as entanglement transition

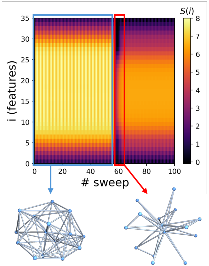

# Features extraction in magnetization patterns

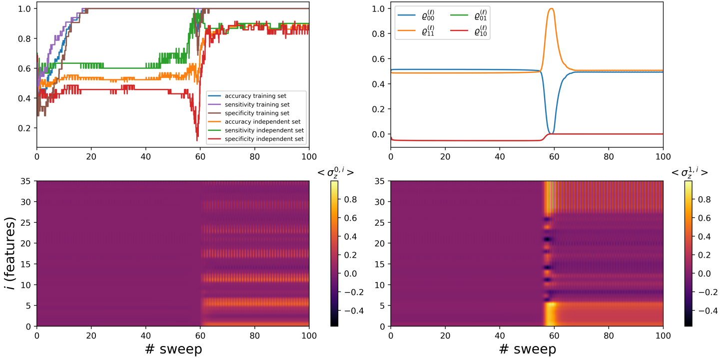

# Features extraction in magnetization patterns

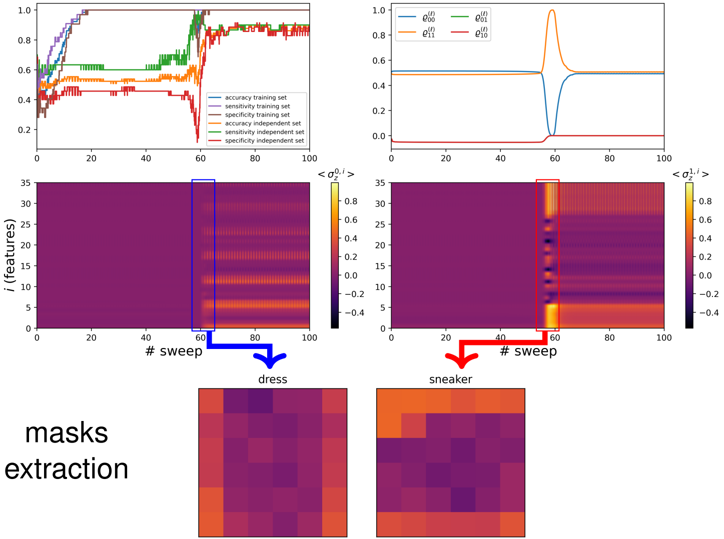

# Entanglement transition

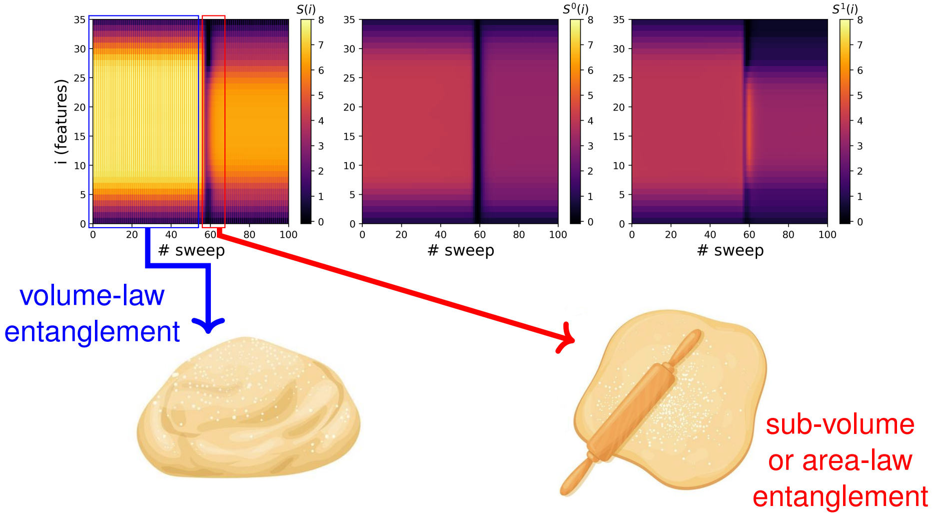

# Entanglement transition

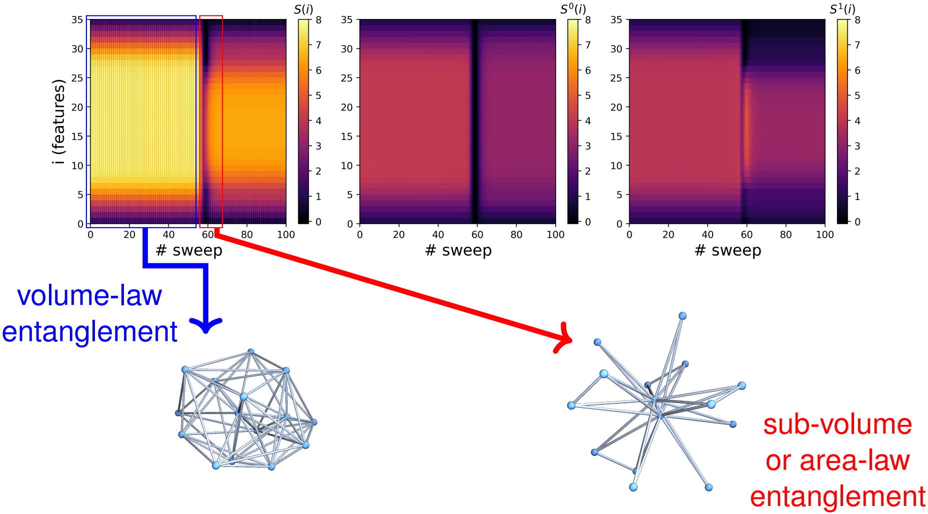

# Outline

- Tensor Networks
  - Matrix Product State (MPS)
  - Gradient descent
- Fashion MNIST
  - Features extraction in magnetization patterns
  - Entanglement transition
- Gene communities
  - Dataset & workflow
  - MPS classification

# Hepatocellular carcinoma (HCC) classification

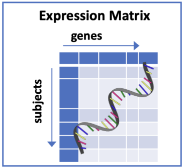


$$r_{ij} = \frac{\sum_{a=1}^{N}(i_a - \bar{i})\sum_{b=1}^{N}(j_b - \bar{j})}{\sqrt{\sum_{a=1}^{N}(i_a - \bar{i})^2}\sqrt{\sum_{b=1}^{N}(j_b - \bar{j})^2}}$$

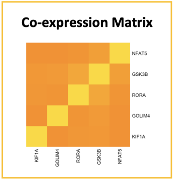


hierarchical clustering: 46 stable communities C1, . . . , C46

Training set: GSE102079 Dataset 140 samples (83 HCC)

Independent set: GSE54236 Dataset with 161 samples (81 HCC)

| | # genes | | # genes | | # genes | | # genes |
|---|---|---|---|---|---|---|---|
| C8 | 28 | C17 | 26 | C29 | 48 | C35 | 31 |
| C12 | 47 | C23 | 31 | C30 | 32 | C40 | 29 |
| C14 | 31 | C24 | 23 | C31 | 25 | C41 | 48 |
| C15 | 25 | C27 | 36 | C32 | 35 | C42 | 33 |
| C16 | 34 | C28 | 35 | C33 | 35 | C43 | 32 |

Lacalamita *et al.*, Artificial Intelligence and Complex Network Approaches Reveal Potential Gene Biomarkers for Hepatocellular Carcinoma, Int. J. Mol. Sci. 24 (2023)

# Flowchart

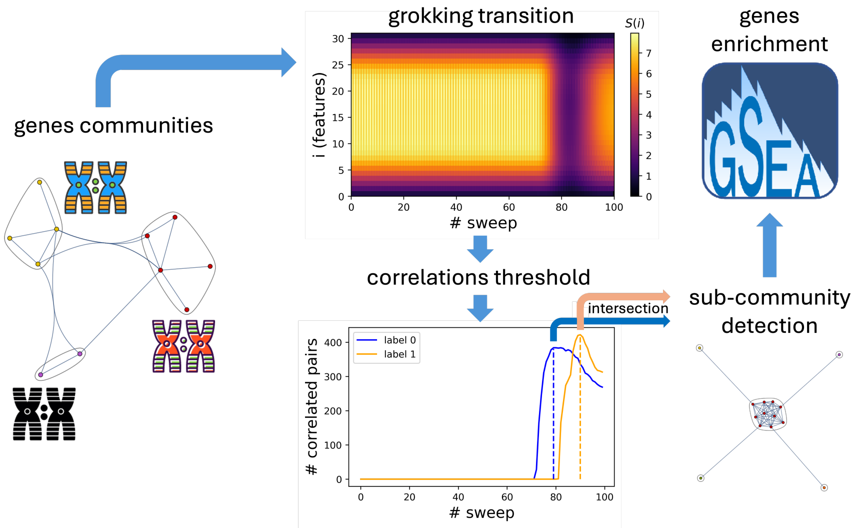
genes communities
grokking transition
S(i)
i (features)
# sweep
genes enrichment
GSEA
correlations threshold
intersection
sub-community detection
label 0
label 1
# correlated pairs
# sweep

# Biologically meaningful gene communities: C29

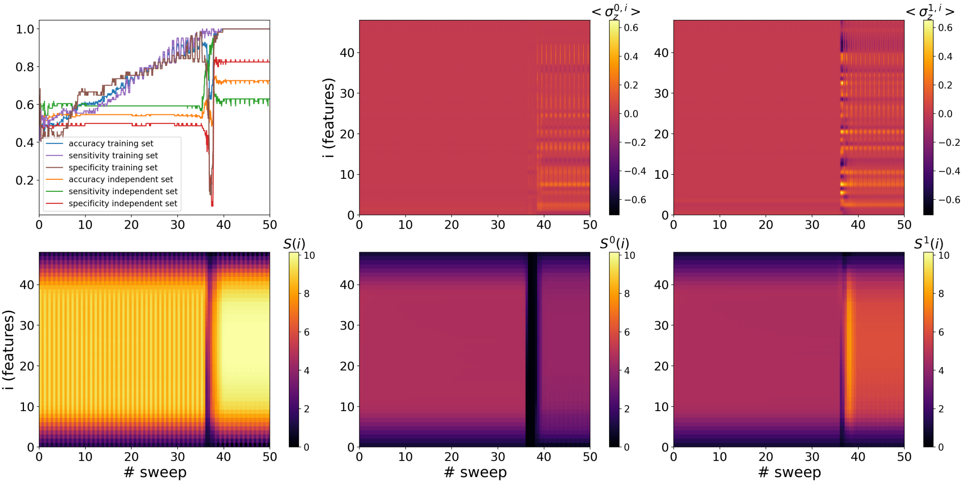

# Biologically meaningful gene communities: C41

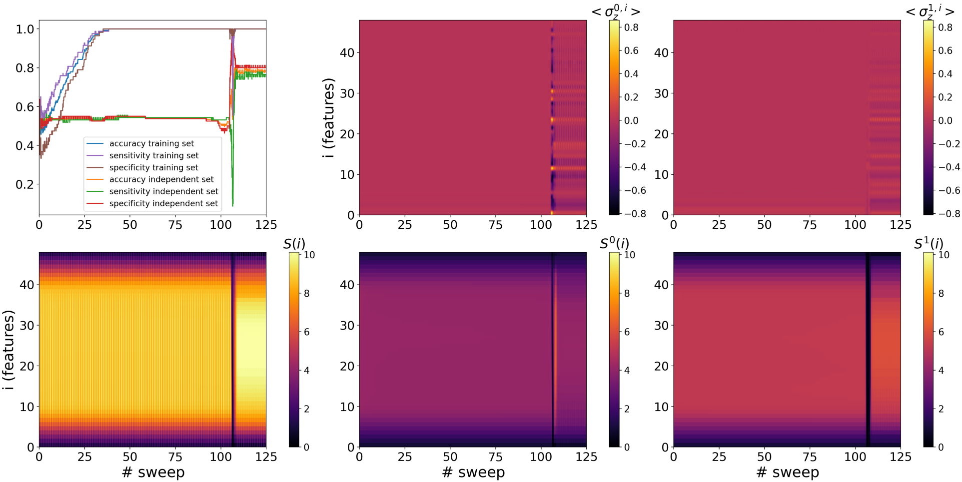

# Volume to sub-volume law entanglement transition

## Left boundary: $\log S = q + c \log i$

| | transition slope | transition $R^2$ | initial slope | initial $R^2$ | final slope | final $R^2$ |
|---|---|---|---|---|---|---|
| C8 | 0.991 | 0.972 | 0.972 | 0.999 | 0.704 | 0.997 |
| C12 | 0.700 | 0.987 | 0.988 | 1.000 | 0.771 | 0.998 |
| C14 | 0.823 | 0.967 | 0.969 | 0.999 | 0.602 | 0.997 |
| C15 | 0.656 | 0.992 | 0.971 | 0.999 | 0.640 | 0.998 |
| C16 | 0.426 | 0.982 | 0.970 | 0.999 | 0.606 | 0.995 |
| C17 | 0.595 | 0.997 | 0.971 | 0.999 | 0.612 | 0.997 |
| C23 | 0.579 | 0.963 | 0.962 | 0.999 | 0.628 | 0.998 |
| C24 | 0.611 | 0.943 | 0.890 | 0.989 | 0.570 | 0.999 |
| C27 | 0.849 | 0.974 | 0.972 | 0.999 | 0.754 | 0.998 |
| C28 | 0.852 | 0.989 | 0.989 | 1.000 | 0.635 | 0.999 |
| C29 | 0.986 | 0.982 | 0.987 | 1.000 | 0.760 | 0.997 |
| C30 | 0.538 | 0.980 | 0.972 | 0.999 | 0.564 | 0.996 |
| C31 | 0.602 | 0.982 | 0.970 | 0.999 | 0.611 | 0.997 |
| C32 | 0.789 | 0.989 | 0.971 | 0.999 | 0.575 | 0.993 |
| C33 | 0.876 | 0.976 | 0.970 | 0.999 | 0.641 | 0.998 |
| C35 | 0.708 | 0.994 | 0.970 | 0.999 | 0.618 | 0.998 |
| C40 | 0.408 | 0.971 | 0.979 | 0.999 | 0.557 | 0.999 |
| C41 | 0.611 | 0.979 | 0.989 | 1.000 | 0.757 | 0.997 |
| C42 | 0.469 | 0.956 | 0.970 | 0.999 | 0.626 | 0.997 |
| C43 | 0.492 | 0.944 | 0.971 | 0.999 | 0.634 | 0.998 |

## Right boundary: $\log S = q + c \log(N - i)$

| | transition slope | transition $R^2$ | initial slope | initial $R^2$ | final slope | final $R^2$ |
|---|---|---|---|---|---|---|
| C8 | 0.686 | 0.995 | 0.938 | 0.997 | 0.630 | 0.999 |
| C12 | 1.004 | 0.972 | 0.974 | 0.999 | 0.761 | 0.996 |
| C14 | 0.453 | 0.991 | 0.934 | 0.997 | 0.597 | 0.996 |
| C15 | 0.919 | 0.991 | 0.937 | 0.997 | 0.639 | 0.997 |
| C16 | 0.701 | 0.986 | 0.935 | 0.997 | 0.620 | 0.996 |
| C17 | 0.835 | 0.977 | 0.937 | 0.997 | 0.626 | 0.998 |
| C23 | 0.765 | 0.968 | 0.920 | 0.994 | 0.611 | 0.997 |
| C24 | 0.728 | 0.981 | 0.794 | 0.973 | 0.496 | 0.995 |
| C27 | 0.668 | 0.995 | 0.942 | 0.997 | 0.674 | 0.997 |
| C28 | 0.670 | 0.987 | 0.972 | 0.999 | 0.669 | 0.998 |
| C29 | 0.714 | 0.966 | 0.972 | 0.999 | 0.759 | 0.999 |
| C30 | 0.873 | 0.990 | 0.939 | 0.997 | 0.604 | 0.995 |
| C31 | 0.806 | 0.995 | 0.938 | 0.997 | 0.633 | 0.996 |
| C32 | 0.654 | 0.962 | 0.934 | 0.997 | 0.566 | 0.998 |
| C33 | 0.961 | 0.918 | 0.936 | 0.997 | 0.620 | 1.000 |
| C35 | 0.766 | 0.989 | 0.939 | 0.997 | 0.604 | 0.996 |
| C40 | 0.656 | 0.943 | 0.939 | 0.997 | 0.601 | 0.997 |
| C41 | 0.726 | 0.965 | 0.973 | 0.999 | 0.769 | 0.993 |
| C42 | 0.715 | 0.986 | 0.935 | 0.997 | 0.631 | 0.996 |
| C43 | 0.701 | 0.971 | 0.935 | 0.997 | 0.612 | 0.995 |

# New enriched gene sub-communities

| | C8 | C12 | C14 | C15 | C16 | C17 | C23 | C24 | C27 | C28 | C29 | C30 | C31 | C32 | C33 | C35 | C40 | C41 | C42 | C43 |
|---|---|---|---|---|---|---|---|---|---|---|---|---|---|---|---|---|---|---|---|---|
| **accuracy** | 0.60 | 0.63 | 0.48 | 0.58 | 0.66 | 0.58 | 0.77 | 0.68 | 0.57 | 0.75 | 0.73 | 0.68 | 0.68 | 0.60 | 0.67 | 0.71 | 0.65 | 0.78 | 0.65 | 0.61 |
| **sensitivity** | 0.41 | 0.41 | 0.57 | 0.56 | 0.58 | 0.43 | 0.69 | 0.53 | 0.59 | 0.63 | 0.63 | 0.65 | 0.77 | 0.56 | 0.59 | 0.69 | 0.49 | 0.75 | 0.49 | 0.65 |
| **specificity** | 0.79 | 0.86 | 0.39 | 0.60 | 0.75 | 0.72 | 0.85 | 0.84 | 0.54 | 0.86 | 0.82 | 0.70 | 0.59 | 0.64 | 0.75 | 0.74 | 0.80 | 0.80 | 0.81 | 0.56 |

Correlation: $C^k_{i,j} = \left(\langle \sigma_Z^{k,i}\sigma_Z^{k,j}\rangle - \langle \sigma_Z^{k,i}\rangle \langle \sigma_Z^{k,j}\rangle\right) / \varrho^{(\ell)}_{k,k}, |C^k_{i,j}| < t, t \in [0,1],$ step $0.1$

# New enriched gene sub-communities

| | C8 | C12 | C14 | C15 | C16 | C17 | C23 | C24 | C27 | C28 | C29 | C30 | C31 | C32 | C33 | C35 | C40 | C41 | C42 | C43 |
|---|---|---|---|---|---|---|---|---|---|---|---|---|---|---|---|---|---|---|---|---|
| **accuracy** | 0.60 | 0.63 | 0.48 | 0.58 | 0.66 | 0.58 | 0.77 | 0.68 | 0.57 | 0.75 | 0.73 | 0.68 | 0.68 | 0.60 | 0.67 | 0.71 | 0.65 | 0.78 | 0.65 | 0.61 |
| **sensitivity** | 0.41 | 0.41 | 0.57 | 0.56 | 0.58 | 0.43 | 0.69 | 0.53 | 0.59 | 0.63 | 0.63 | 0.65 | 0.77 | 0.56 | 0.59 | 0.69 | 0.49 | 0.75 | 0.49 | 0.65 |
| **specificity** | 0.79 | 0.86 | 0.39 | 0.60 | 0.75 | 0.72 | 0.85 | 0.84 | 0.54 | 0.86 | 0.82 | 0.70 | 0.59 | 0.64 | 0.75 | 0.74 | 0.80 | 0.80 | 0.81 | 0.56 |

Correlation: $C^k_{i,j} = \left( \langle \sigma_Z^{k,i} \sigma_Z^{k,j} \rangle - \langle \sigma_Z^{k,i} \rangle \langle \sigma_Z^{k,j} \rangle \right) / \varrho^{(\ell)}_{k,k},\ |C^k_{i,j}| < t,\ t \in [0,1],$ step $0.1$

| **C16** | **C29** | **C41** |
|---|---|---|
| GOBP_NEGATIVE_REGULATION_OF_WNT_SIGNALING_PATHWAY | GOBP_AMEBOIDAL_TYPE_CELL_MIGRATION | GOBP_POSITIVE_REGULATION_OF_INTRACELLULAR_SIGNAL_TRANSDUCTION |
| GOBP_OSSIFICATION | GOBP_EMBRYONIC_PLACENTA_MORPHOGENESIS | GOBP_CELL_CHEMOTAXIS |
| GOBP_HEART_MORPHOGENESIS | GOBP_MORPHOGENESIS_OF_AN_EPITHELIAL_FOLD | GOBP_NEGATIVE_REGULATION_OF_RESPONSE_TO_STIMULUS |
| GOMF_GLYCOSAMINOGLYCAN_BINDING | GOBP_NEURAL_TUBE_FORMATION | REACTOME_CLASS_B_2_SECRETIN_FAMILY_RECEPTORS |
| GOBP_CELL_CELL_SIGNALING_BY_WNT | GOBP_ODONTOGENESIS_OF_DENTIN_CONTAINING_TOOTH | REACTOME_GPCR_LIGAND_BINDING |
| GOBP_POSITIVE_REGULATION_OF_NERVOUS_SYSTEM_DEVELOPMENT | GOBP_NEGATIVE_REGULATION_OF_KERATINOCYTE_PROLIFERATION | GOMF_SIGNALING_RECEPTOR_REGULATOR_ACTIVITY |
| GOBP_NEGATIVE_REGULATION_OF_CANONICAL_WNT_SIGNALING_PATHWAY | GOBP_REGULATION_OF_CANONICAL_WNT_SIGNALING_PATHWAY | GOBP_TUBE_MORPHOGENESIS |
| GOBP_SKELETAL_SYSTEM_DEVELOPMENT | GOBP_IN_UTERO_EMBRYONIC_DEVELOPMENT | GOBP_NEGATIVE_REGULATION_OF_MULTICELLULAR_ORGANISMAL_PROCESS |
| WNT_SIGNALING | GOBP_LABYRINTHINE_LAYER_MORPHOGENESIS | GOBP_NEGATIVE_REGULATION_OF_VIRAL_ENTRY_INTO_HOST_CELL |
| **C28** | WP_ANGIOGENESIS | GOBP_INFLAMMATORY_RESPONSE |
| GOBP_COMPLEMENT_ACTIVATION_LECTIN_PATHWAY | GOBP_METANEPHRIC_GLOMERULUS_DEVELOPMENT | GOBP_POSITIVE_REGULATION_OF_SIGNALING |
| KEGG_COMPLEMENT_AND_COAGULATION_CASCADES | GOBP_MESENCHYMAL_CELL_DIFFERENTIATION | GOBP_RESPONSE_TO_POTASSIUM_ION |
| GOBP_COMPLEMENT_ACTIVATION | KEGG_MEDICUS_REFERENCE_REGULATION_OF_GF_RTK_RAS_ERK_SIGNALING_UBIQUITINATION_OF_RTK_BY_CBL | GOBP_MAPK_CASCADE |
| KEGG_FOLATE_BIOSYNTHESIS | GOBP_GLAND_DEVELOPMENT | GOBP_SKELETAL_SYSTEM_DEVELOPMENT |
| **C30** | GOBP_MALE_GENITALIA_DEVELOPMENT | REACTOME_PLATELET_ACTIVATION_SIGNALING_AND_AGGREGATION |
| GOCC_VACUOLE | GOBP_RESPONSE_TO_ALCOHOL | GOMF_PROTEIN_CONTAINING_COMPLEX_BINDING |
| GOBP_MONONUCLEAR_CELL_MIGRATION | **C35** | GOMF_HORMONE_BINDING |
| GOBP_REGULATION_OF_BLOOD_PRESSURE | GOBP_PURINERGIC_NUCLEOTIDE_RECEPTOR_SIGNALING_PATHWAY | REACTOME_HEMOSTASIS |
| GOBP_MACROPHAGE_CHEMOTAXIS | GOBP_MATURE_B_CELL_DIFFERENTIATION_INVOLVED_IN_IMMUNE_RESPONSE | REACTOME_ERYTHROCYTES_TAKE_UP_CARBON_DIOXIDE_AND_RELEASE_OXYGEN |
| GOBP_CELLULAR_RESPONSE_TO_OXYGEN_CONTAINING_COMPOUND | GOBP_POSITIVE_REGULATION_OF_MOLECULAR_FUNCTION | WP_GPCRS_CLASS_B_SECRETINLIKE |
| KEGG_FOCAL_ADHESION | GOBP_MONOATOMIC_ION_TRANSPORT | GOCC_SECRETORY_GRANULE |
| GOBP_MONOATOMIC_CATION_TRANSMEMBRANE_TRANSPORT | GOBP_POSITIVE_REGULATION_OF_PEPTIDYL_TYROSINE_PHOSPHORYLATION | REACTOME_G_ALPHA_S_SIGNALLING_EVENTS |
| GOBP_REGULATION_OF_CELL_CELL_ADHESION | GOBP_NEGATIVE_REGULATION_OF_LYMPHOCYTE_ACTIVATION | GOBP_CELL_ACTIVATION |
| WP_MIRNA_TARGETS_IN_ECM_AND_MEMBRANE_RECEPTORS | **C40** | GOBP_RESPONSE_TO_OXYGEN_CONTAINING_COMPOUND |
| REACTOME_DISEASES_ASSOCIATED_WITH_GLYCOSAMINOGLYCAN_METABOLISM | GOMF_LYASE_ACTIVITY | GOBP_ACTIVATION_OF_IMMUNE_RESPONSE |
| PID_FRA_PATHWAY | GOBP_GENERATION_OF_PRECURSOR_METABOLITES_AND_ENERGY | |

# Conclusions

- Monitoring the training dynamics allows us to identify critical behaviors influencing generalization properties;
- MPS classifiers are able to manage high computational complexity and highlight local magnetization for each “mask” trained per class;
- Grokking implies an entanglement phase transition, but the viceversa does not hold true;
- Correlations allow us to identify gene sub-communities endowed with enriched gene sets.

# Conclusions

- Monitoring the training dynamics allows us to identify critical behaviors influencing generalization properties;
- MPS classifiers are able to manage high computational complexity and highlight local magnetization for each “mask” trained per class;
- Grokking implies an entanglement phase transition, but the viceversa does not hold true;
- Correlations allow us to identify gene sub-communities endowed with enriched gene sets.

Thank you!

Questions/Comments?

# Gradient descent

Two sites update:

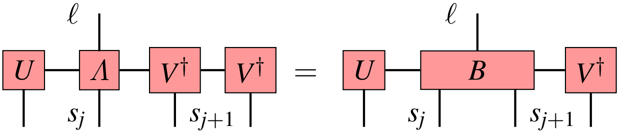


single right step, leading to a sweep when back at the initial sites pair.

Stoudenmire, Schwab, Supervised Learning with Tensor Networks, 2016

## Gradient descent

Two sites update:

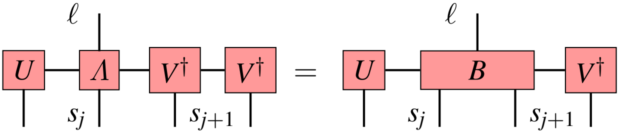


single right step, leading to a sweep when back at the initial sites pair.

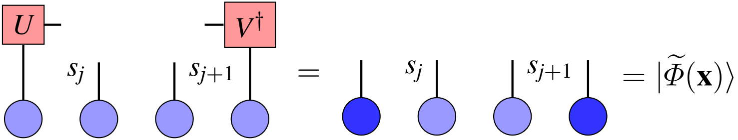


$$f_W^\ell(\mathbf{x}) = \sum_{s_j, s_{j+1}} \sum_{a_{j-1}, a_{j+1}} B^{a_{j-1}, \ell, a_{j+1}}_{s_j, s_{j+1}} \, |\widetilde{\Phi}(\mathbf{x})^{s_j, s_{j+1}}_{a_{j-1}, a_{j+1}}\rangle$$

Stoudenmire, Schwab, Supervised Learning with Tensor Networks, 2016

# Gradient descent

Two sites update:

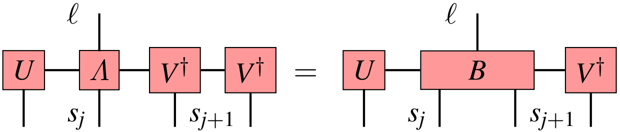


single right step, leading to a sweep when back at the initial sites pair.

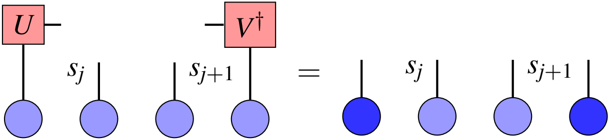


$= |\widetilde{\Phi}(\mathbf{x})\rangle$

$$f_W^{\ell}(\mathbf{x}) = \sum_{s_j, s_{j+1}} \sum_{a_{j-1}, a_{j+1}} B^{a_{j-1}, \ell, a_{j+1}}_{s_j, s_{j+1}} |\widetilde{\Phi}(\mathbf{x})^{s_j, s_{j+1}}_{a_{j-1}, a_{j+1}}\rangle$$

$$\Delta B^{\ell} = -\frac{\partial \mathcal{C}}{\partial B^{\ell}} = \sum_{\omega=1}^{N_T} |\widetilde{\Phi}(\mathbf{x}_\omega)\rangle \otimes (y_\omega^{\ell} - f_W^{\ell}(\mathbf{x}_\omega)) \quad \Longrightarrow \quad B'^{\ell} = B^{\ell} + \alpha \Delta B^{\ell}$$

---

Stoudenmire, Schwab, Supervised Learning with Tensor Networks, 2016

# Measured observables

- Reduced density matrix:

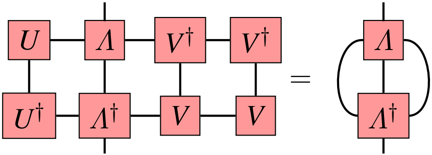


$$= \varrho^{(\ell)} = \begin{pmatrix} \varrho_{00}^{(\ell)} & \varrho_{01}^{(\ell)} \\ \varrho_{10}^{(\ell)} & \varrho_{11}^{(\ell)} \end{pmatrix}$$

# Measured observables

- Reduced density matrix:

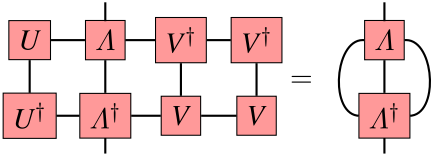


$$= \varrho^{(\ell)} = \begin{pmatrix} \varrho_{00}^{(\ell)} & \varrho_{01}^{(\ell)} \\ \varrho_{10}^{(\ell)} & \varrho_{11}^{(\ell)} \end{pmatrix}$$

- Local magnetization $\langle \sigma_Z^{k,i} \rangle, k = 0, 1$:

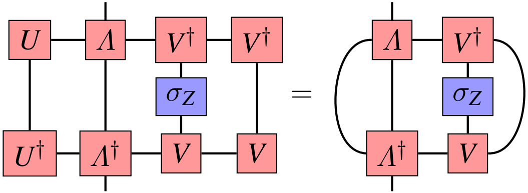

# Measured observables

- Reduced density matrix:

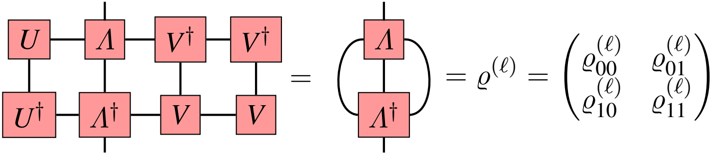


- Local magnetization $\langle \sigma_Z^{k,i} \rangle, k = 0, 1$:

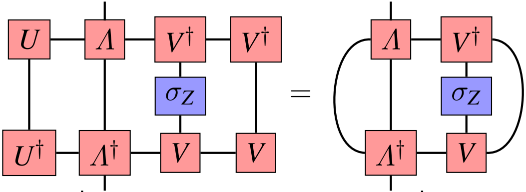


- Correlation function $\langle \sigma_Z^{k,i} \sigma_Z^{k,j} \rangle, k = 0, 1$:

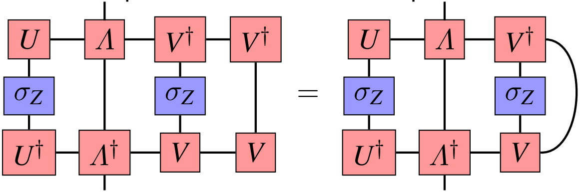

# Binary sneaker classifications entropies

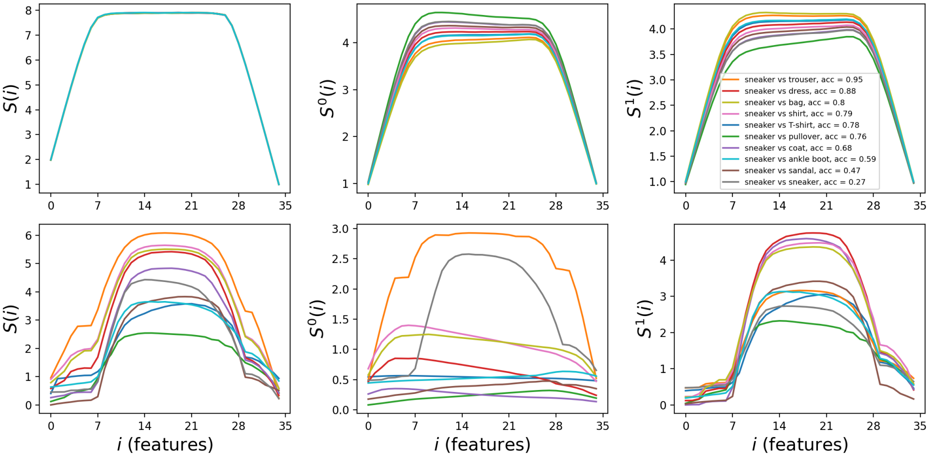

# Entanglement transition

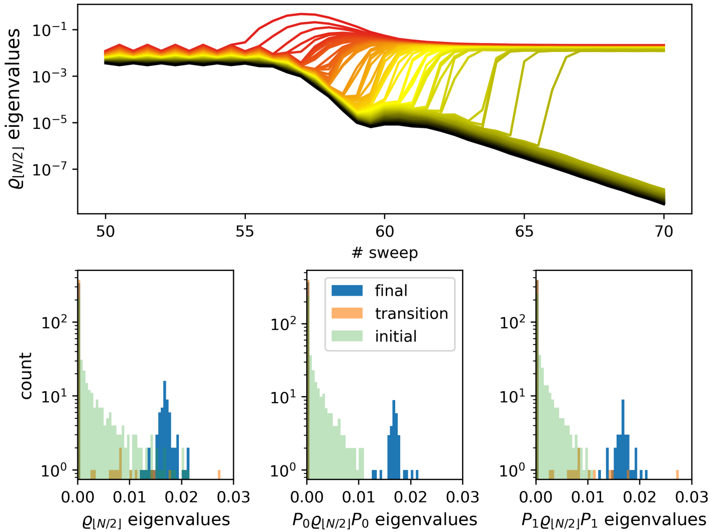

# Fake classification sneaker vs sneaker with coherence

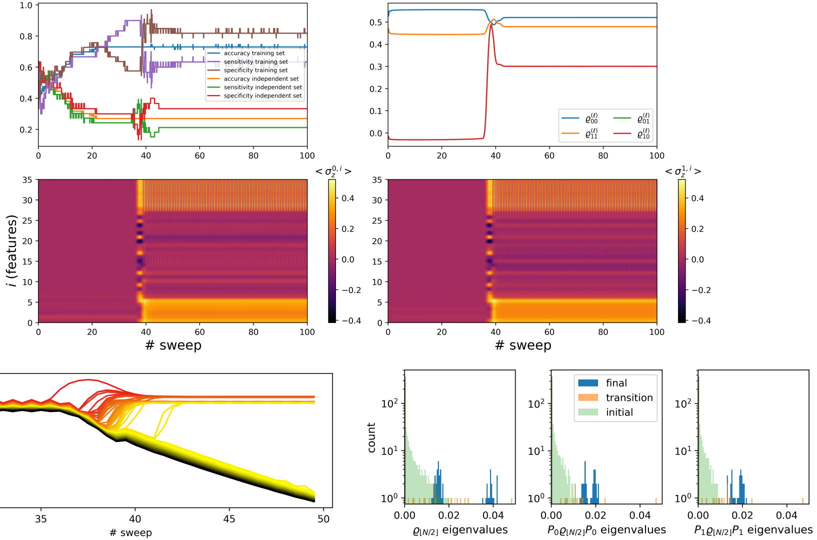

# Hepatocellular carcinoma (HCC) classification

GSE102079
Dataset
257 samples
(152 HCC)

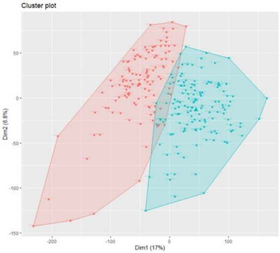


| | Cluster 1 | Cluster 2 |
|---|---|---|
| Normal + Peritumoral | 100 | 5 |
| HCC | 20 | 132 |

# Hepatocellular carcinoma (HCC) classification

GSE102079
Dataset
257 samples
(152 HCC)

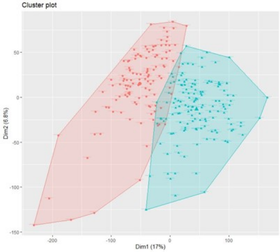


| | Cluster 1 | Cluster 2 |
|---|---|---|
| Normal + Peritumoral | 100 | 5 |
| HCC | 20 | 132 |

MPS
classification

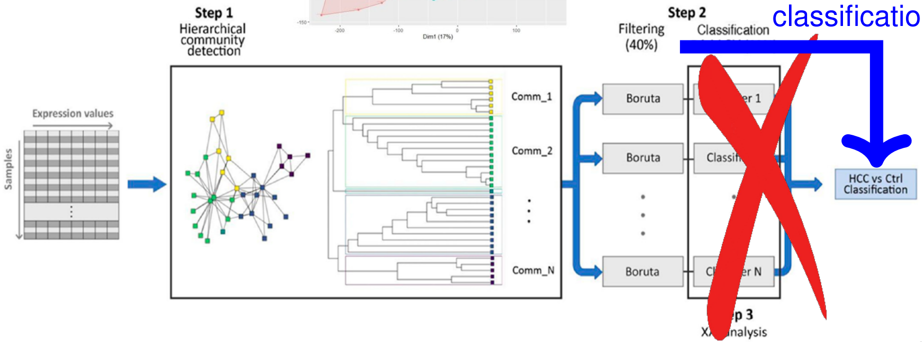

# MPS correlations for gene community C23

Optimal permutation of features:

$$C^k_{i,j} = \frac{\langle \sigma_Z^{k,i} \sigma_Z^{k,j} \rangle - \langle \sigma_Z^{k,i} \rangle \langle \sigma_Z^{k,j} \rangle}{\varrho^{(\ell)}_{k,k}}$$

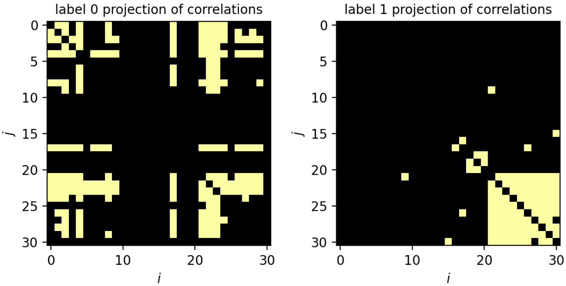


selected pairs
$|C^k_{i,j}| > 0.5$

Decreased bond dimension: $400 \to 300$, still showing magnetization after $\approx 30$ sweeps

# Volume to sub-volume law entanglement transition

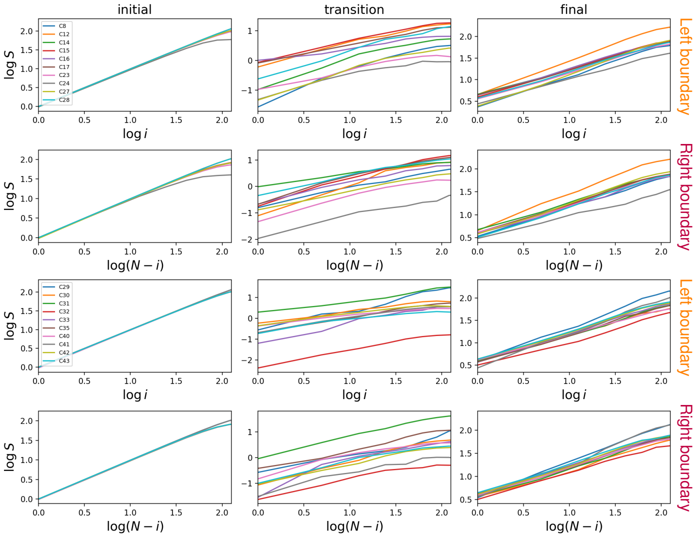

# Eigenvalues evaporation and correlations

C29

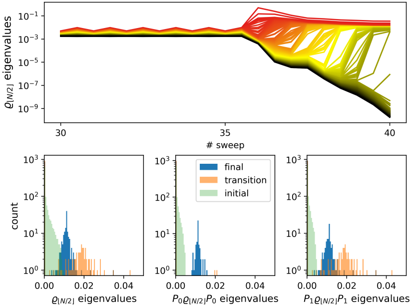


C41

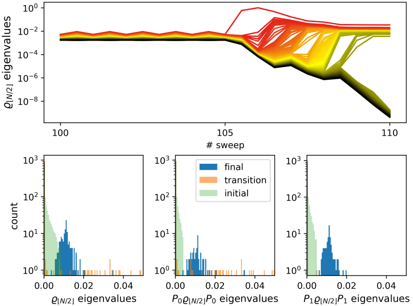

# Eigenvalues evaporation and correlations

C29

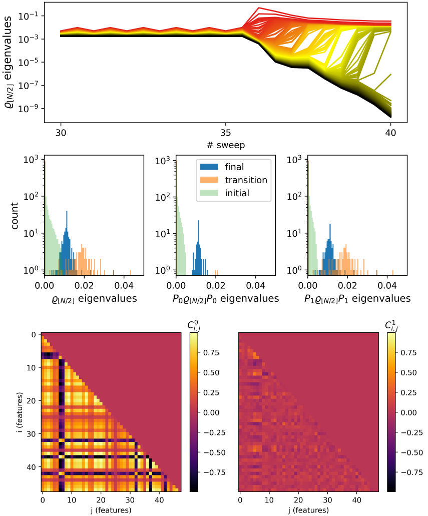


C41